

Original Article

Epidural Pulsation Accelerates the Drainage of Brain Interstitial Fluid

Xianjie Cai^{1,2,3}, Qingyuan He², Wei Wang⁴, Chunlin Li⁵, Hui Wang^{1,3}, Feng Yin⁶, Tong Li⁶, Dongsheng Kong⁷, Yanxing Jia⁸, Hongfeng Li¹, Junhao Yan⁹, Xunbin Wei¹, Qiushi Ren^{1,10}, Yajuan Gao^{2,3}, Shuangfeng Yang¹¹, Huaiyu Tong^{7*}, Yun Peng^{11*}, Hongbin Han^{1,2,3,12*}

¹Institute of Medical Technology, Peking University Health Science Center, Beijing, China. ²Department of Radiology, Peking University Third Hospital, Beijing, China. ³Beijing Key Laboratory of Magnetic Resonance Imaging Equipment and Technique, Beijing, China. ⁴Department of Radiology, Beijing Rehabilitation Hospital, Capital Medical University, Beijing, China. ⁵School of Biomedical Engineering, Capital Medical University, Beijing, China. ⁶Department of Neurosurgery, Aerospace Center Hospital, Peking University Aerospace Clinical College, Beijing, China. ⁷Department of Neurosurgery, First Medical Center, General Hospital of Chinese PLA, Beijing, China. ⁸State Key Laboratory of Natural and Biomimetic Drugs, School of Pharmaceutical Sciences, Peking University, Beijing, China. ⁹Department of Anatomy and Histology, School of Basic Medical Sciences, Peking University, Beijing, China. ¹⁰Department of Biomedical Engineering, College of Future Technology, Peking University, Beijing, China. ¹¹Department of Radiology, Beijing Children's Hospital, Capital Medical University, National Center for Children's Health, Beijing, China. ¹²Institute of Biomedical Engineering, Peking University Shenzhen Graduate School, Shenzhen, China.

[Received February 22, 2022; Revised June 8, 2022; Accepted June 9, 2022]

ABSTRACT: Unhindered transportation of substances in the brain extracellular space (ECS) is essential for maintaining brain function. Regulation of transportation is a novel strategy for treating ECS blockage-related brain diseases, but few techniques have been developed to date. In this study, we established a novel approach for accelerating the drainage of brain interstitial fluid (ISF) in the ECS using minimally invasive surgery, in which a branch of the external carotid artery is separated and implanted epidurally (i.e., epidural arterial implantation [EAI]) to promote a pulsation effect on cerebrospinal fluid (CSF) in the frontoparietal region. Tracer-based magnetic resonance imaging was used to evaluate the changes in ISF drainage in rats 7 and 15 days post-EAI. The drainage of the traced ISF from the caudate nucleus to ipsilateral cortex was significantly accelerated by EAI. Significant increases in the volume fraction of the ECS and molecular diffusion rate were demonstrated using the D_{ECS} -mapping technique, which may account for the mechanisms underlying the changes in brain ISF. This study provides a novel perspective for encephalopathy treatment via the brain ECS.

Key words: extracellular space, interstitial fluid, cerebrospinal fluid, MRI, brain

Due to the absence of a lymphatic system in the brain [1], substance transport and elimination of metabolic waste rely predominantly on interstitial fluid (ISF) drainage. Perturbations of ISF drainage may cause abnormal

deposition of substances in the brain extracellular space (ECS), resulting in brain dysfunction such as Alzheimer's disease (AD) [2-4], stroke [5, 6], and epilepsy [7]. Accordingly, improving brain ISF drainage has been

*Correspondence should be addressed to: Dr. Hongbin Han, Peking University Third Hospital, Beijing, China. Email: hanhongbin@bjmu.edu.cn; Dr. Huaiyu Tong, First Medical Center, General Hospital of Chinese PLA, Beijing, China. Email: tongh215@163.com; Dr. Yun Peng, Beijing Children's Hospital, Capital Medical University, National Center for Children's Health, Beijing, China. Email: ppengyun@yahoo.com.

Copyright: © 2022 Cai X. et al. This is an open-access article distributed under the terms of the [Creative Commons Attribution License](https://creativecommons.org/licenses/by/4.0/), which permits unrestricted use, distribution, and reproduction in any medium, provided the original author and source are credited.

proposed as a promising therapeutic strategy for brain diseases [1, 8-10]. Our previous study verified that the deposition of amyloid β ($A\beta$) protein in the AD brain leads to ECS blockage and a reduction in ISF drainage, and red light at 630 nm disrupts $A\beta$ deposition in the ECS and recovers ISF flow accompanied by reversed memory in an AD animal model [11]. Hence, the artificial and active regulation of brain ISF drainage to promote the clearance of toxins from the brain ECS is a promising strategy for treating brain diseases.

Substance transport in the brain ECS is influenced by multiple factors. Maturation of the myelin sheath determines the direction and rate of ISF drainage from the caudate nucleus (Cn) to the ipsilateral superficial cortex [12]. Brain ISF drains bidirectionally from the Cn toward the cortex and thalamus in juvenile rats. In contrast, in the adult brain, it drains only toward the ipsilateral cortex along the mature myelin sheath [12, 13]. The exchange of ISF-cerebrospinal fluid (CSF) occurs in the superficial cortex with the assistance of arterial pulsation and then enters the subarachnoid space (SAS) [14], which then drains to the deep cervical lymph nodes via the epidural lymph vessels and flows into the somatic circulation [15]. The release of excitatory transmitters after neuronal excitation in the thalamus secondary to nociceptive stimulation leads to restricted diffusion in the ECS [16], which can result in downregulation of brain ISF drainage in the thalamus.

Based on recent findings regarding the drainage pathway and influencing factors, we hypothesized that ISF drainage may be accelerated by a change in local CSF flow. To test this theory, we achieved local arterial pulsation effects by implanting a separate arterial branch of the external carotid artery in the space between the dura and skull, and CSF acceleration enhanced the exchange of CSF-ISF, thereby altering ISF drainage in the brain parenchyma. Tracer-based magnetic resonance imaging (MRI) [17] was employed to measure alterations in ISF drainage from the Cn in rats on days 7 and 15 after epidural arterial implantation (EAI) surgery. The D_{ECS} mapping technique [18] was applied to quantitatively analyze ECS structure and molecular diffusion changes in the Cn region to clarify the microstructural basis of altered ISF drainage by EAI. Further, we discuss the significance of accelerating ISF drainage for the treatment of neurological disorders.

MATERIALS AND METHODS

Experimental animals

Experiments were performed on adult male Sprague-Dawley rats (8 weeks old, weighing 250–300 g). The animal experimental protocol was approved by the Peking

University Biomedical Ethics Committee (permit number: LA20200335). Animals were housed under a 12-hour light/dark diurnal cycle, temperature of $22\pm 1^\circ\text{C}$, and humidity of $60\pm 5\%$. Animals were provided *ad libitum* access to food and clean drinking water [13].

Rats were randomly divided into six groups according to the surgical procedure and time interval between the experimental operation and surgery: the EAI groups (EAI 7 and EAI 15 groups), control groups (Con 7 and Con 15 groups), EAI contralateral measurement group (EAI-C7 group), and EAI plus gelatin sponge pad group (EAI-G7 group) ($n = 12$ per group for Morris water maze (MWM), $n = 6$ per group for other experiments).

Epidural arterial implantation

EAI surgery: After induction of anesthesia using intraperitoneal injection of a combination of pentobarbital sodium (Sigma, St. Louis, MO, USA); ethanol (Zhenyuminsheng Pharmaceutical Company, Beijing, China); chloral hydrate (Sigma), magnesium sulfate (Zhenyuminsheng Pharmaceutical Company); and propylene glycol (Zhenyuminsheng Pharmaceutical Company) (0.3 mL/kg) [17], each rat was placed in the prone position, and the right periotic region was shaved. The scope for shaving was positioned anterior to the area between the eyes, posterior to the neck, left of the central line, and right to approximately 1 cm below the ear. Under the microscope, the skin was cut perpendicular to the external auditory canal using microsurgery forceps and scissors to expose the temporalis. An “L”-shaped turn was made anteriorly to completely expose the temporalis and part of the skull on the top of the head. The superficial temporal artery was completely dissociated along the course of the blood vessels, fine branches were disconnected, and peripheral fascia was preserved. After dissociation, the skull at the top of the head was removed using a craniotomy drill. The skull window was extended vertically, with a length and width of approximately 2 and 1 cm, respectively. The dura was exposed along the long axis. After surgery, the skin was sutured using dislocation and relaxation sutures such that the dissociated superficial temporal artery covered the dura mater. The remaining soft tissues on both sides of the blood vessels were sutured to the residual periosteal margins on both sides, and the skin was sutured using a whole-layer suture. The skin was sterilized by wiping with iodophor, indicating completion of surgery. An illustration of the EAI surgery procedure is presented in Figure 1.

EAI plus subvascular gelatin sponge pad procedure: The procedure was performed in the same manner as that for the EAI surgical group. After exposing the intact dura, a piece of gelatin sponge (Xiang En Medical Technology Development Company, Beijing, China), approximately

0.5×0.5 cm in size, was carefully placed on the dura. The artery was then placed on a gelatin sponge. The skin was

sterilized by wiping with iodophor, indicating the completion of surgery.

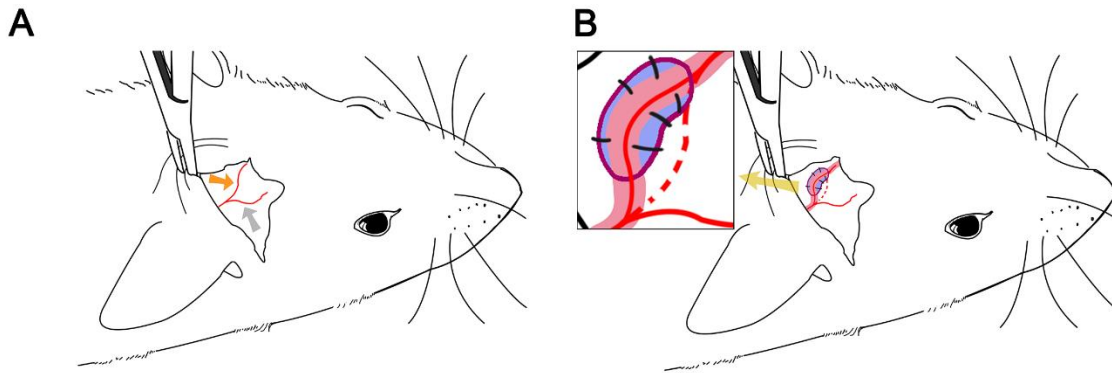


Figure 1. Illustration of EAI surgery. (A) The upper epidermis of the rat ear was cut, and the superficial fascia was exposed. The parietal branch (orange arrow) and frontal branch (gray arrow) of the superficial temporal artery were visible. (B) Magnification of surgery area (pointed to by yellow arrow) was shown in the top-left of the image. After the superficial temporal artery (red) and the surrounding soft tissue (pink) were successfully dissociated, the dura mater (blue) was exposed by drilling in the adjacent parietal bone area. The superficial temporal artery was affixed to the dura mater and the suture line (black line) was used to suture the soft tissue around the superficial temporal artery and the skull periosteum (purple line).

Sham surgery: After induction of anesthesia by intraperitoneal injection of compound anesthesia, each rat was placed in the prone position, and the right periotic region was shaved. The scope was placed anterior to the area between the eyes, posterior to the neck, left of the central line, and right to approximately 1 cm below the ear. The intact dura was exposed along the long axis. The skin was sterilized by wiping with iodophor, indicating the completion of surgery.

Intracranial tracer injection: Gadolinium diethyltriaminepentaacetic acid (Gd-DTPA)-enhanced MRI scanning technology, independently invented by our laboratory, was used to measure the distribution of the contrast agent in the brain ECS. Gd-DTPA (10 mmol/L, Magnevist; Bayer Schering Pharma AG, Berlin, Germany) was diluted to 10 mmol/L in 154 mmol/L NaCl solution and injected into the Cn. Rats were administered compound anesthesia. After induction of anesthesia, rats were scanned using MRI to determine the location of the injection site and then placed in a stereotaxic-single frame (Lab Standard Stereotaxic-Single; Stoelting Co., Wood Dale, IL, USA) for complete fixation. After surgical exposure of the skull, the skull was drilled according to the desired location, and Gd-DTPA was injected into the right Cn (AP: 1 mm, L: -3 mm, V: -6 mm) using a microinjection pump. For rats in the EAI-C group, Gd-DTPA was injected into the left Cn (AP: 1 mm; L: 3 mm; V: -6 mm). After correct placement of the 10- μ L microsyringe (Hamilton Bonaduz AG, Bonaduz, Switzerland), the injection parameters of the syringe pump (Harvard Equipment, Holliston, MA, USA) were adjusted to deliver a total injection volume of 2 μ L at an injection rate of 0.2 μ L/min. After injection of the contrast

agent, the needle was left in place for 10 min to prevent backflow of the contrast agent along the needle track. After 10 min, the needle was withdrawn at a uniform speed over the course of 5 min.

Tracer-based MRI scanning

Images were acquired using an MRI scanner (Magnetom Trio, Siemens Medical Solutions, Erlangen, Germany) equipped with a dedicated coil for small animals. Images of the rat brain were obtained using T1-weighted magnetization for rapid acquisition of gradient-echo sequences. The acquisition parameters were set as follows: echo time, 3.7 ms; repetition time, 1,500 ms; flip angle, 9°; inversion time, 900 ms; field of view, 267 mm; voxel size, 0.5 mm³; matrix, 512 × 512; average, 2; and phase-encoding step, 96. The acquisition time was 290 s for each rat each time point. All rats were scanned before and after tracer administration. The scan time points were pre-injection scans and 15, 30, 45, 60, 90, 120, 150, 180, and 240 min post-injection. Tracer-based MRI scans were performed on rats in the Con 7, EAI 7, EAI-C7, and EAI-G7 groups on the 7th day after surgery and on rats in the Con15 and EAI15 groups on the 15th day after surgery.

Brain ISF drainage and brain ECS parameter acquisition and analysis

Imaging data were processed using the Nano-Detect Analysis System software, as previously described (MRI Lab, Beijing, China) [18, 19]. All images were initially processed with grayscale calibration and histogram equalization. Subsequently, post-injection images were

compared with the baseline image for image registration. Rigid transformation, mutual information measurements, high-order interpolation, and adaptive stochastic gradient descent optimization were used to achieve an accurate image registration. The images were then subtracted from the pre-scanned images. The "bright regions" obtained by creating a seed point and threshold in the region of interest were considered relevant to the tracer. A new set of post-processed MRI images was created in the horizontal, sagittal, and coronal planes. The software generated new MRI images in the horizontal, sagittal, and coronal planes, with a slice thickness of 1 mm.

The equivalent diffusion coefficient for each MRI image pixel in the vicinity of the injection site (1–2 mm from the injection site) was derived using a modified diffusion equation. The volume fraction (α) was defined as the ECS volume fraction of the entire brain tissue. Tortuosity (λ) was defined as D/D^* , where D^* was the effective diffusion coefficient of a given molecule in the brain ECS, D was the diffusion coefficient of the same molecule in a free medium, and λ was the hindrance of diffusion by the local ECS structure [14]. The obtained ECS microstructure parameters included α , λ , and D^* .

Physiological parameter acquisition

The heart and respiratory rates of the rats were acquired using an MR-compatible small animal monitoring and gating system (Model 1030, Small Animal Instruments, Inc., NY, USA). Measurements were made on rats in the Con 7, EAI 7, EAI-C7, and EAI-G7 groups on the 7th day post-surgery.

Animals were anesthetized as described above and were placed on the test bench. Detection needles were inserted into the two front paws and right rear paw, and a heart rate detection patch was placed on the abdomen of the rats. After commencement of measurements, data were recorded after the measurements had stabilized, and the heart and respiratory rates of the rats were recorded every 30 min. The total monitoring duration was 2 h.

Weights and local cerebral blood flow in the surgical area of rats in the Con 7, EAI 7, EAI-C7, and EAI-G7 groups (i.e., the same rats used for MRI scanning) were acquired using a balance scale (ZS-DZC, Zhongshi Dichuang Technology Development Co., Ltd., Beijing, China) and laser Doppler flowmetry (LDF, Moor VMS-LDF2, UK), respectively, pre-surgery and 7 days post-surgery.

After exposure of the intact dura during surgery, a VP4 probe of the LDF instrument was positioned approximately 1 mm from the dura. Measurements were obtained continuously for 2 min to collect pre-surgical data. After the artery covered the dura, the VP4 probe was repositioned approximately 1 mm from the dura, and

measurements were obtained continuously for 2 min to collect post-surgical data.

Behavioral and cognitive assessments

A modified neurological severity score (mNSS) test was conducted to evaluate neurological function of rats in the Con 7 and EAI 7 groups pre-surgery and on the 7th day post-surgery. The assessments comprised motor, sensory, reflex, and balance tests, with scores ranging from 0 to 18 (normal score, 0; maximal deficit score, 18). Higher test scores indicated more severe neurological deficits [20, 21].

The MWM test was conducted to assess spatial learning and memory capability of rats in the Con 7 and EAI 7 groups as previously described [13, 22]. On day 1, rats were pretrained to find a visual platform, which was 1 cm above the surface of the water, to adapt to the test procedure. From the 2nd to 5th days, the rats were allocated 60 s and released into water from four starting points in four quadrants. The time taken by the rats to find the hidden platform submerged 1 cm below the water was recorded as the escape latency. After the platform was removed on the 6th day, the rats were released from a randomly determined starting point and allowed to swim for 60 s. The average time to find the platform (escape latency), passing times, and swim path for each rat were recorded. Test parameters were recorded automatically using a video tracking system (Zhongshi Dichuang Technology Development Co., Ltd., Beijing, China).

Statistical analysis

Statistical analyses were performed using SPSS version 26.0 (IBM Corp., Armonk, NY, USA). Data that followed the normal distribution were expressed as the mean \pm standard deviation. Independent-samples t-tests were used for comparisons between two groups; one-way ANOVA and the Bonferroni test were used for comparisons between multiple groups. Two-way ANOVA and the Bonferroni test were used for comparisons of escape latency in MWM. Data that did not follow a normal distribution were expressed as medians and quartiles. Kruskal-Wallis test was used for comparisons between multiple groups. All statistical tests were two-sided, and a p -value < 0.05 was considered statistically significant.

RESULTS

Changes in ISF drainage on the 7th day after EAI

Tracer-based MRI examinations revealed a tracer-labeled, high-brightness ISF from the Cn that gradually drained

along the white matter to the ipsilateral cortex over time and eventually dissipated into the SAS (Fig. 2A).

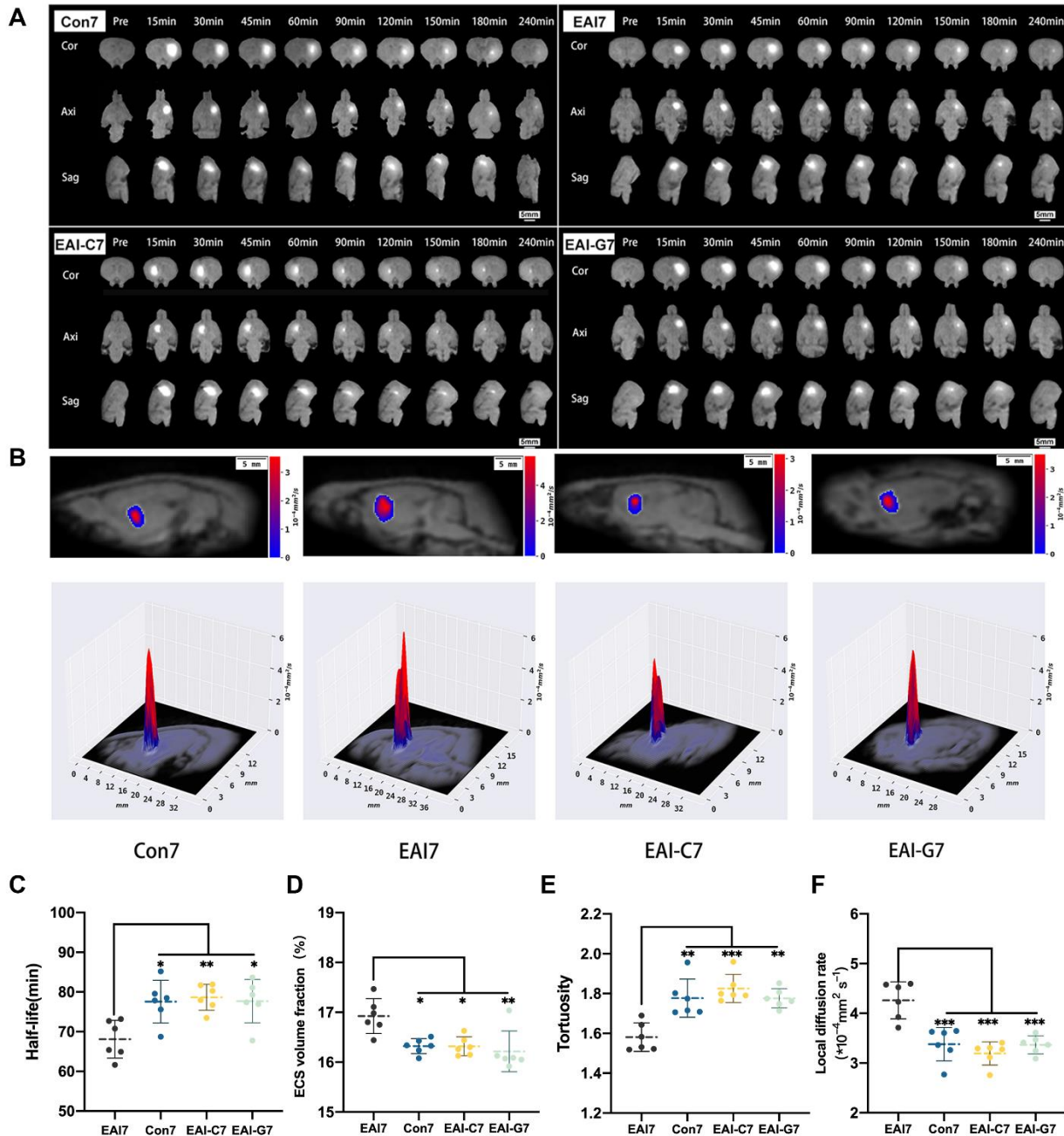


Figure 2. Images and comparison of ISF drainage and ECS structure parameters of rats at day 7. (A) Images of ISF drainage by tracer-based MRI scanning of the Con 7, EAI 7, EAI-C7, and EAI-G7 groups. The tracer injected into the caudate nucleus (highlighted area in the figure) spread with time to the ipsilateral cerebral cortex and eventually dissipated from the brain parenchyma (Cor: coronal image; Axi: axial image; Sag: sagittal image). Scale bar (white) = 5 mm. (B) Two-dimensional and three-dimensional mapping of local diffusion rates in ECS of Con 7, EAI 7, EAI-C7, and EAI-G7 groups. The image shows that the local diffusion rate in the EAI 7 group is higher than that in the Con 7, EAI-C7, and EAI-G7 groups. (C) Half-life of ISF drainage was lower in the EAI 7 group than that in the Con 7, EAI-C7, and EAI-G7 groups. No significant differences were observed in the comparison of the Con 7, EAI-C7, and EAI-G7 groups. D: ECS volume fraction was higher in the EAI 7 group than that in the Con 7, EAI-C7, and EAI-G7 groups. No significant differences were observed in the comparison of the Con 7, EAI-C7, and EAI-G7 groups. (E) ECS tortuosity was lower in the EAI 7 group than that in the Con 7, EAI-C7, and EAI-G7 groups. No significant differences were observed between the Con 7, EAI-C7, and EAI-G7 groups. F: Local diffusion rate in the ECS was higher in the EAI 7 group than that in the Con 7, EAI-C7, and EAI-G7 groups. No significant differences were found between the Con 7, EAI-

C7, and EAI-G7 groups. Kruskal-Wallis test was used for comparisons of ECS volume fraction, ANOVA with Bonferroni test was used for comparisons of other parameters, $n = 6$ per group. * $p < 0.05$, ** $p < 0.01$, *** $p < 0.001$ compared to the EAI 7 group. Con 7: control group (7 days); EAI 7: epidural arterial implantation group (7 days); EAI-C7: epidural arterial implantation-contralateral measurement group (7 days); EAI-G7: epidural arterial implantation-gelatin sponge group (7 days); ISF, interstitial fluid; ECS, extracellular space

Compared with the Con 7, EAI-C7, and EAI-G7 groups, the EAI 7 group exhibited faster ISF drainage from the Cn to ipsilateral cortex via the white matter (EAI 7 vs Con 7: 68.10 ± 4.75 min vs 77.57 ± 5.38 min, $p < 0.05$; EAI 7 vs EAI-C7: 68.10 ± 4.75 min vs 78.66 ± 3.20 min, $p < 0.01$; EAI 7 vs EAI-G7: 68.10 ± 4.75 min vs

77.69 ± 5.45 min, $p < 0.05$, Bonferroni test, $n = 6$). No significant difference was observed in the comparison of brain ISF drainage between the Con 7, EAI-C7, and EAI-G7 groups (77.57 ± 5.38 min vs 78.66 ± 3.20 min vs 77.69 ± 5.45 min, $p > 0.05$, Bonferroni test, $n = 6$) (Table 1, Fig. 2C).

Table 1. Comparison of ISF drainage and ECS structure on the 7th and 15th day after EAI ($n = 6$ per group).

Time	Group	T _{1/2} (min)	α (%)	λ	D* ($\times 10^{-4}$ mm ² /s)
Day 7	EAI 7	68.10 ± 4.75	16.93 ± 0.35	1.58 ± 0.70	4.26 ± 0.37
	Con 7	$77.57 \pm 5.38^*$	$16.32 \pm 0.15^*$	$1.78 \pm 0.10^{**}$	$3.38 \pm 0.34^{***}$
	EAI-C7	$78.66 \pm 3.20^{**}$	$16.32 \pm 0.19^*$	$1.83 \pm 0.71^{***}$	$3.19 \pm 0.23^{***}$
	EAI-G7	$77.69 \pm 5.45^*$	$16.08(16.01, 16.36)^{**}$	$1.78 \pm 0.48^{**}$	$3.37 \pm 0.18^{***}$
Day 15	EAI15	67.42 ± 7.98	16.99 ± 0.63	1.56 ± 0.86	4.41 ± 0.49
	Con15	$78.03 \pm 8.35^{\#}$	$16.16 \pm 0.08^{\#}$	$1.78 \pm 0.55^{###}$	$3.36 \pm 0.21^{\#}$

Compared to the Con 7, EAI-C7, and EAI-G7 groups, the EAI 7 group exhibited accelerated ISF drainage, expanded brain ECS, decreased tortuosity, and enhanced diffusion rate in the ECS of the Cn. Compared to the Con15 group, the EAI15 group exhibited accelerated ISF drainage, expanded brain ECS, decreased tortuosity, and enhanced diffusion rate in the ECS of the Cn. No statistically significant difference was noted between the EAI 7 and EAI15 groups. Kruskal-Wallis test was used for comparisons of ECS volume fraction; ANOVA with Bonferroni test was used for comparisons of other parameters, $n = 6$ per group. * $p < 0.05$, ** $p < 0.01$, *** $p < 0.001$ compared to EAI 7 group; $^{\#}p < 0.05$, $^{###}p < 0.001$ compared to EAI15 group. Con 7, control group (7 days); EAI 7, epidural arterial implantation group (7 days); EAI-C7, epidural arterial implantation-contralateral measurement group (7 days); EAI-G7, epidural arterial implantation-gelatin sponge group (7 days); Con15, control group (15 days); EAI15, epidural arterial implantation group (15 days); ISF, interstitial fluid; ECS, extracellular space; Cn, caudate nucleus

Changes in brain ECS on the 7th day after EAI

D_{ECS} mapping revealed alterations in the ECS structure and local diffusion rate within the ECS of Cn (Fig. 2B). Compared with the Con 7, EAI-C7, and EAI-G7 groups, the EAI 7 group exhibited a higher volume fraction of brain ECS [EAI 7 vs Con 7: $16.93 \pm 0.35\%$ vs $16.32 \pm 0.15\%$, $p < 0.05$; EAI 7 vs EAI-C7: $16.93 \pm 0.35\%$ vs $16.32 \pm 0.19\%$, $p < 0.05$; EAI 7 vs EAI-G7: $16.93 \pm 0.35\%$ vs 16.08% (16.01%, 16.36%), $p < 0.01$, Kruskal-Wallis test, $n = 6$]. No significant differences were observed in the volume fraction of ECS between the Con 7, EAI-C7, and EAI-G7 groups [$16.32 \pm 0.15\%$ vs $16.32 \pm 0.19\%$ vs 16.08% (16.01%, 16.36%), $p > 0.05$, Kruskal-Wallis test, $n = 6$] (Table 1, Fig. 2D).

Compared to the Con 7, EAI-C7, and EAI-G7 groups, the EAI 7 group exhibited lower ECS tortuosity in the Cn (EAI 7 vs Con 7: 1.58 ± 0.70 vs 1.78 ± 0.10 , $p < 0.01$; EAI 7 vs EAI-C7: 1.58 ± 0.70 vs 1.83 ± 0.70 , $p < 0.001$; EAI 7 vs EAI-G7: 1.58 ± 0.70 vs 1.78 ± 0.48 , $p < 0.01$; Bonferroni test, $n = 6$). There was no difference in the comparison of ECS tortuosity between the Con 7, EAI-C7 and EAI-G7 groups (1.78 ± 0.10 vs 1.83 ± 0.70 vs 1.78 ± 0.48 , $p > 0.05$, Bonferroni test, $n = 6$) (Table 1, Fig. 2E).

Compared to the Con 7, EAI-C7, and EAI-G7 groups, the EAI 7 group exhibited a higher local diffusion rate in the Cn region (EAI 7 vs Con 7: 4.26 ± 0.37 vs $3.38 \pm 0.34 \times 10^{-4} / \text{mm}^2$, $p < 0.001$; EAI 7 vs EAI-C7: 4.26 ± 0.37 vs $3.19 \pm 0.23 \times 10^{-4} / \text{mm}^2$, $p < 0.001$; EAI 7 vs EAI-G7: $4.26 \pm 0.37 \times 10^{-4} / \text{mm}^2$ vs 3.37 ± 0.181 , $p < 0.001$, Bonferroni test, $n = 6$). No significant differences were observed in the comparison of local diffusion rate within the ECS between the Con 7, EAI-C7, and EAI-G7 groups (3.38 ± 0.34 vs 3.19 ± 0.23 vs $3.37 \pm 0.181 \times 10^{-4} / \text{mm}^2$, $p > 0.05$, Bonferroni test, $n = 6$) (Table 1, Fig. 2F).

Changes to physiological and neurobehavioral function after EAI

No significant differences were observed in respiratory and heart rates on the 7th day post-surgery or in the weights and local cerebral blood flow pre-surgery and 7 days post-surgery between the Con 7, EAI 7, EAI-C7, and EAI-G7 groups ($p > 0.05$, Bonferroni test, $n = 6$) (Fig. 3A-D, Supplementary Tables 1-3).

The mNSS and MWM tests were performed to investigate the effects of EAI surgery on neurological function. In the mNSS test, scores of all rats in the Con 7

and EAI 7 groups were zero, and no significant differences were observed in the escape latency ($p > 0.05$, Bonferroni test, $n = 6$ for the mNSS test, $n = 12$ for the MWM test) (Fig. 3E-G, Supplementary Table 4) and

passing times (Con 7 vs EAI 7: 2.75 ± 1.76 vs 2.25 ± 1.48 , $p > 0.05$, t-test, $n = 12$) (Fig. 3H, Supplementary Table 4) between the Con 7 and EAI 7 groups.

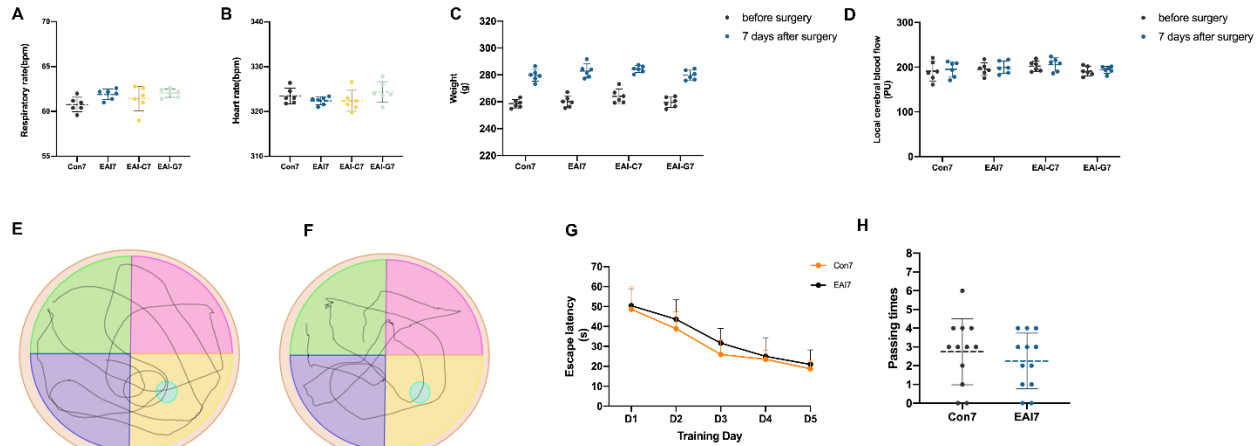


Figure 3. Comparison of physiological and neurobehavioral function parameters. (A-B) No significant differences were observed in respiratory and heart rates between the Con 7, EAI-C7, and EAI-G7 groups on the 7th day post-surgery. (C-D) No significant differences were observed in weights and local cerebral blood flow before and 7 days after surgery between the Con 7, EAI 7, EAI-C7, and EAI-G7 groups. (E) Tracks in the Morris water maze tests of Con 7 group. (F) Tracks in the Morris water maze tests of EAI 7 group. (G) The escape latency of the rats during a five-day period. No significant differences were observed between the Con 7 and EAI 7 groups. (H) No significant differences were observed in number of platform crossings between the Con 7 and EAI 7 groups. One-way ANOVA analysis with Bonferroni test and Kruskal-Wallis test for comparisons of respiratory rates, heart rates, weights, and local cerebral blood flow, two-way ANOVA analysis with Bonferroni test for comparisons of escape latency in MWM, and independence-samples t-test for comparisons of passing times in MWM. Con 7: control group (7 days); EAI 7: epidural arterial implantation group (7 days); EAI-C7: epidural arterial implantation-contralateral measurement group (7 days); EAI-G7: epidural arterial implantation-gelatin sponge group (7 days); MWM, Morris water maze.

Stability analysis of EAI in the regulation of brain ISF drainage and substance transport in brain ECS

To further identify the stability of the surgical efficacy of EAI, we supplemented the analysis of brain ISF drainage and ECS structural parameters in rats in the EAI and control groups 15 days post-surgery (Table 1). Compared with the Con15 group, the EAI15 group exhibited faster ISF drainage (67.42 ± 7.98 min vs 78.03 ± 8.35 min, $p < 0.05$, t-test, $n = 6$) (Fig. 4A), a higher volume fraction of brain ECS ($16.99 \pm 0.63\%$ vs $16.16 \pm 0.08\%$, $p < 0.05$, t-test, $n = 6$) (Fig. 4B), lower ECS tortuosity in the Cn region (1.56 ± 0.86 vs 1.78 ± 0.55 , $p < 0.001$, t-test, $n = 6$) (Fig. 4C), and enhanced local diffusion (4.41 ± 0.49 vs $3.36 \pm 0.21 \times 10^{-4}/\text{mm}^2$, $p < 0.05$, t-test, $n = 6$) (Fig. 4D). No significant differences were observed in the comparison of brain ISF drainage (68.10 ± 4.75 min vs 67.42 ± 7.975 min, $p > 0.05$, t-test, $n = 6$), brain ECS volume fraction ($16.93 \pm 0.35\%$ vs $16.99 \pm 0.63\%$, $p > 0.05$, t-test, $n = 6$), tortuosity (1.58 ± 0.70 vs 1.56 ± 0.86 , $p > 0.05$, t-test, $n = 6$), and local diffusion rate within the ECS (4.26 ± 0.37 vs $4.41 \pm 0.49 \times 10^{-4}/\text{mm}^2$, $p > 0.05$, t-test, $n = 6$) between the EAI 7 and EAI15 groups (Table

1, Fig. 4E-H). These results indicated that brain ISF drainage and ECS structure could be artificially and actively regulated by EAI. In particular, the enhancement effect of ISF was stable over a relatively long time.

DISCUSSION

In this study, we established a minimally invasive method for the active modulation of cerebral ISF drainage. Epidural implantation of an external carotid artery branch resulted in accelerated ISF drainage from the Cn to the ipsilateral cortex. The elasticity and integrity of dura under EAI ensured an efficient pulsation effect on the CSF and resulted in a long-term and stable accelerated ISF drainage.

During the EAI procedure, a free branch of the external carotid artery was placed on the dura in the frontoparietal region, below which the ISF drained from the Cn, reaching the SAS to communicate with the CSF. After arriving at the CSF, the tracer molecules moved more rapidly owing to a local synchronized pulsatile compression from the implanted artery, which led to an increase in the local concentration gradient of tracer

molecules between the ISF and CSF. The increase in local concentration gradient enhanced the concentration-driven diffusion of the tracer molecules from the brain ECS to CSF, which presented as an increased ISF drainage and diffusion rate. Meanwhile, acceleration of ISF drainage and ECS diffusion was accompanied by a widening of the ECS and a decrease in tortuosity. ECS contains extracellular matrix and numerous inorganic and organic molecules [8, 14]. Recent studies have shown that both the volume fraction and diffusion rate can be regulated by

chemical changes in the brain ECS. Previous studies have shown that different anesthetics as well as neuronal activities could change the volume fraction of the brain ECS with the release of norepinephrine or glutamic acid in the brain [16, 23]. Other studies found that endogenous formaldehyde could affect ISF drainage in the brain ECS due to A β deposition [11, 24, 25]. Substance variation in the brain ECS under EAI and its potential influence on the brain ECS structure warrants further investigation.

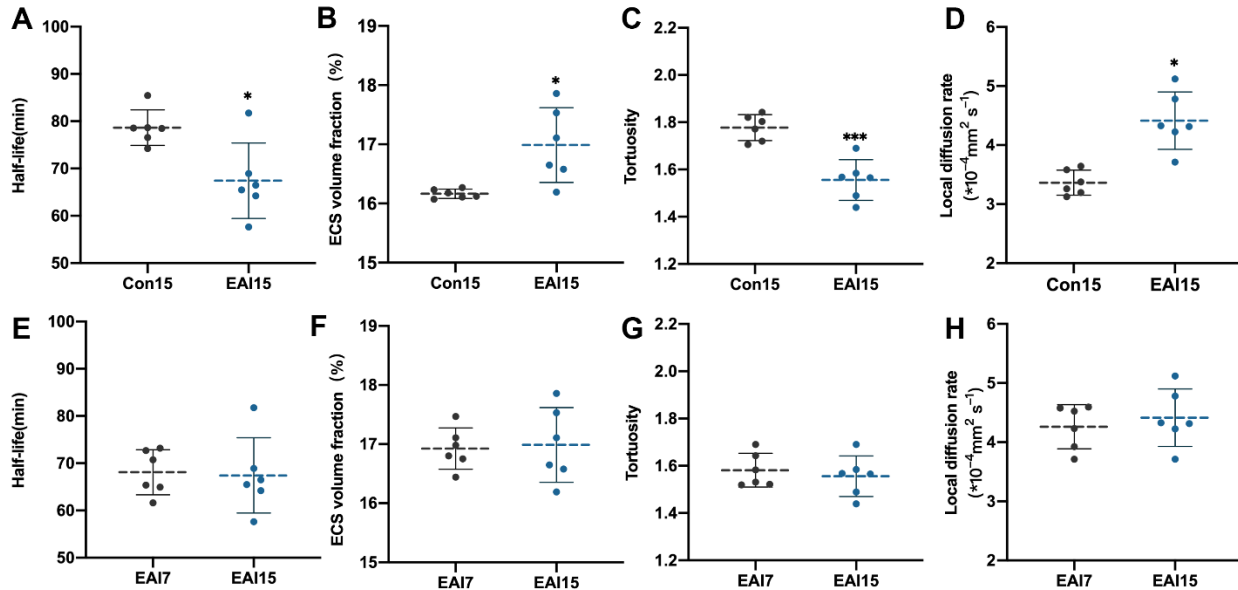


Figure 4. Comparison of ISF drainage and ECS structure at days 7 and 15. (A-D) Compared with the Con15 group, the EAI 15 group exhibited faster ISF drainage, higher volume fraction of brain ECS, lower ECS tortuosity, and enhanced local diffusion in Cn. (E-H) No significant differences were observed in the comparison of brain ISF drainage and ECS structural changes between the EAI 7 and EAI 15 groups in ISF drainage and ECS structure. Independent-samples t-test, $n = 6$ per group. * $p < 0.05$, *** $p < 0.001$ compared to EAI 7 group. Con 7, control group (7 days); Con 15, control group (15 days), EAI 7: epidural arterial implantation group (7 days); EAI 15, epidural arterial implantation group (15 days); ISF, interstitial fluid; ECS, extracellular space.

A growing body of research indicates that abnormal deposition of materials in the brain ECS is closely associated with various brain diseases. AD is the most common cause of dementia [26]. In AD, A β peptides aggregate into amyloid oligomers and plaques and are involved in AD pathogenesis [27]. Indeed, impaired clearance of A β within the brain ECS is closely associated with AD [3]. Epilepsy is a disorder in which the brain experiences recurrent, abnormal, synchronous excitatory activity in a population of neurons that manifests as behavioral seizures. In epilepsy disorders, a moderate increase in the extracellular K⁺ concentration can enhance epileptiform activity [7]. The accumulation of proinflammatory cytokines in the brain ECS of ischemic stroke has long-term toxic effects on cortical and hippocampal neurons [28]. The safe, stable, and long-term effect of EAI on accelerating ISF drainage highlights the

promising value of EAI in the treatment of these ECS blockage-related brain diseases.

Acknowledgments

We would like to thank Wenjie Liao from the Institute of Medical Technology, Peking University Health Science Center for his help with illustration editing. This work was supported by the National Major Scientific Research Instrument Development Project (61827808), National Natural Science Foundation of China (12171330), Summit Program of Foshan (2019B008) and Shenzhen Science and Technology Program (KQTD2018041218 1221912).

Competing interests

The authors declare that they have no conflict of interest.

Supplementary Materials

The Supplementary data can be found online at:
www.aginganddisease.org/EN/10.14336/AD.2022.0609.

References

- [1] Rasmussen MK, Mestre H, Nedergaard M (2018). The glymphatic pathway in neurological disorders. *Lancet Neurol*, 17:1016-1024.
- [2] Tarasoff-Conway JM, Carare RO, Osorio RS, Glodzik L, Butler T, Fieremans E, et al. (2015). Clearance systems in the brain-implications for Alzheimer disease. *Nat Rev Neurol*, 11:457-470.
- [3] Weller RO, Subash M, Preston SD, Mazanti I, Carare RO (2008). Perivascular drainage of amyloid-beta peptides from the brain and its failure in cerebral amyloid angiopathy and Alzheimer's disease. *Brain Pathol*, 18:253-266.
- [4] Reeves BC, Karimy JK, Kundishora AJ, Mestre H, Cerci HM, Matouk C, et al. (2020). Glymphatic System Impairment in Alzheimer's Disease and Idiopathic Normal Pressure Hydrocephalus. *Trends Mol Med*, 26:285-295.
- [5] Hrabetová S, Hrabe J, Nicholson C (2003). Dead-space microdomains hinder extracellular diffusion in rat neocortex during ischemia. *J Neurosci*, 23:8351-8359.
- [6] Schain AJ, Melo-Carrillo A, Strassman AM, Burstein R (2017). Cortical Spreading Depression Closes Paravascular Space and Impairs Glymphatic Flow: Implications for Migraine Headache. *J Neurosci*, 37:2904-2915.
- [7] Perkins KL, Arranz AM, Yamaguchi Y, Hrabetova S (2017). Brain extracellular space, hyaluronan, and the prevention of epileptic seizures. *Rev Neurosci*, 28:869-892.
- [8] Shetty AK, Zanirati G (2020). The Interstitial System of the Brain in Health and Disease. *Aging Dis*, 11:200-211.
- [9] Bobo RH, Laske DW, Akbasak A, Morrison PF, Dedrick RL, Oldfield EH (1994). Convection-enhanced delivery of macromolecules in the brain. *Proc Natl Acad Sci U S A*, 91:2076-2080.
- [10] Han H, Xia Z, Chen H, Hou C, Li W (2011). Simple diffusion delivery via brain interstitial route for the treatment of cerebral ischemia. *Sci China Life Sci*, 54:235-239.
- [11] Yue X, Mei Y, Zhang Y, Tong Z, Cui D, Yang J, et al. (2019). New insight into Alzheimer's disease: Light reverses A β -obstructed interstitial fluid flow and ameliorates memory decline in APP/PS1 mice. *Alzheimers Dement (N Y)*, 5:671-684.
- [12] Wang A, Wang R, Cui D, Huang X, Yuan L, Liu H, et al. (2019). The Drainage of Interstitial Fluid in the Deep Brain is Controlled by the Integrity of Myelination. *Aging Dis*, 10:937-948.
- [13] Wang R, Han H, Shi K, Alberts IL, Rominger A, Yang C, et al. (2021). The Alteration of Brain Interstitial Fluid Drainage with Myelination Development. *Aging Dis*, 12:1729-1740.
- [14] Lei Y, Han H, Yuan F, Javeed A, Zhao Y (2017). The brain interstitial system: Anatomy, modeling, in vivo measurement, and applications. *Prog Neurobiol*, 157:230-246.
- [15] Aspelund A, Antila S, Proulx ST, Karlsten TV, Karaman S, Detmar M, et al. (2015). A dural lymphatic vascular system that drains brain interstitial fluid and macromolecules. *J Exp Med*, 212:991-999.
- [16] Li Y, Han H, Shi K, Cui D, Yang J, Alberts IL, et al. (2020). The Mechanism of Downregulated Interstitial Fluid Drainage Following Neuronal Excitation. *Aging Dis*, 11:1407-1422.
- [17] Han H, Shi C, Fu Y, Zuo L, Lee K, He Q, et al. (2014). A novel MRI tracer-based method for measuring water diffusion in the extracellular space of the rat brain. *IEEE J Biomed Health Inform*, 18:978-983.
- [18] Gao Y, Han H, Du J, He Q, Jia Y, Yan J, et al. (2021). Early changes to the extracellular space in the hippocampus under simulated microgravity conditions. *Sci China Life Sci*.
- [19] Teng Z, Wang A, Wang P, Wang R, Wang W, Han H (2018). The Effect of Aquaporin-4 Knockout on Interstitial Fluid Flow and the Structure of the Extracellular Space in the Deep Brain. *Aging Dis*, 9:808-816.
- [20] Bieber M, Gronewold J, Scharf AC, Schuhmann MK, Langhauser F, Hopp S, et al. (2019). Validity and Reliability of Neurological Scores in Mice Exposed to Middle Cerebral Artery Occlusion. *Stroke*, 50:2875-2882.
- [21] Long X, Yao X, Jiang Q, Yang Y, He X, Tian W, et al. (2020). Astrocyte-derived exosomes enriched with miR-873a-5p inhibit neuroinflammation via microglia phenotype modulation after traumatic brain injury. *J Neuroinflammation*, 17:89.
- [22] Liu X, Zhang M, Liu H, Zhu R, He H, Zhou Y, et al. (2021). Bone marrow mesenchymal stem cell-derived exosomes attenuate cerebral ischemia-reperfusion injury-induced neuroinflammation and pyroptosis by modulating microglia M1/M2 phenotypes. *Exp Neurol*, 341:113700.
- [23] Zhao G, Han H, Yang J, Sun M, Cui D, Li Y, et al. (2020). Brain interstitial fluid drainage and extracellular space affected by inhalational isoflurane: in comparison with intravenous sedative dexmedetomidine and pentobarbital sodium. *Sci China Life Sci*, 63:1-17.
- [24] Tong Z, Han C, Luo W, Wang X, Li H, Luo H, et al. (2013). Accumulated hippocampal formaldehyde induces age-dependent memory decline. *Age (Dordr)*, 35:583-596.
- [25] Zhu R, Zhang G, Jing M, Han Y, Li J, Zhao J, et al. (2021). Genetically encoded formaldehyde sensors inspired by a protein intra-helical crosslinking reaction. *Nat Commun*, 12:581.
- [26] Wang M, Jiang J, Yan Z, Alberts I, Ge J, Zhang H, et al. (2020). Individual brain metabolic connectome indicator based on Kullback-Leibler Divergence

- [27] Similarity Estimation predicts progression from mild cognitive impairment to Alzheimer's dementia. *Eur J Nucl Med Mol Imaging*, 47:2753-2764.
- [28] Zbesko JC, Nguyen TV, Yang T, Frye JB, Hussain O, Hayes M, et al. (2018). Glial scars are permeable to the neurotoxic environment of chronic stroke infarcts. *Neurobiol Dis*, 112:63-78.
- [29] Barnhart CD, Yang D, Lein PJ (2015). Using the Morris water maze to assess spatial learning and memory in weanling mice. *PLoS One*, 10:e0124521.
- [27] Grimmer T, Shi K, Diehl-Schmid J, Natale B, Drzezga A, Förster S, et al. (2020). (18)F-FIBT may expand PET for β -amyloid imaging in neurodegenerative diseases. *Mol Psychiatry*, 25:2608-2619.